IEEE Access
Multidisciplinary ⋮ Rapid Review ⋮ Open Access Journal

Received 27 November 2024, accepted 15 January 2025, date of publication 4 February 2025, date of current version 14 February 2025.

Digital Object Identifier 10.1109/ACCESS.2025.3538813

RESEARCH ARTICLE

Power Loss Observations in Algorithmically Designed PMSM Stator Windings Utilizing the Freedoms Afforded by Additive Manufacturing

JOHN MCKAY[1], (Member, IEEE), JILL MISCANDLON[2], AND TATYANA KONKOVA[1]
[1]Department of Design, Manufacturing and Engineering Management, University of Strathclyde, G1 1XJ Glasgow, U.K.
[2]National Manufacturing Institute Scotland, University of Strathclyde, G1 1XJ Glasgow, U.K.

Corresponding author: John McKay (John.mckay@strath.ac.uk)

This work was supported in part by the Industrial Doctorate Centre at the National Manufacturing Institute Scotland, which is part of the University of Strathclyde; and in part by the Engineering and Physical Sciences Research Council of U.K. Future Electrical Machines Manufacturing Hub under Grant EP/S018034/1.

ABSTRACT Permanent magnet synchronous machines (PMSM) are an increasingly popular motor topology for many industries such as automotive, aerospace, manufacturing, energy and premium consumer goods. PMSM offer many advantages compared to other topologies such as induction machines due to their higher power density, greater operational efficiency and high torque, whilst remaining robust and fault tolerant. One specific area of interest is the stator windings. With increasing operational speed, the geometric configuration of the winding becomes ever increasingly important in order to mitigate increasing AC losses. The windings conductor lay in slot, position, shape and orientation become critical in combating loss mechanisms such as skin effect, proximity effect and armature reaction. Additive manufacturing offers a novel geometric design freedom that has previously been unattainable using traditional manufacturing methods and enables the ability to create highly novel winding design methodologies that could potentially revolutionise winding design and performance. This work investigates the losses observed from an algorithmically designed stator winding, additively manufactured in AlSi10Mg using the laser powder bed fusion process. A motorette sub-assembly was constructed and the DC and AC power losses were measured and compared against a theoretical 3D FEA based simulation model. The outcome observed a 9.4% difference in losses comparing theoretical and measured winding values utilising the RAC/RDC measured. Samples of the additively manufactured conductor parts have been tested for resistivity and conductivity.

INDEX TERMS Additive manufacturing, aerospace industry, automotive industry, electric motors, genetic algorithms, optimization, PMSM, stator windings.

I. INTRODUCTION

Permanent magnet synchronous machines (PMSM) are becoming an ever increasingly utilised motor topology across many different industries. Such industries include automotive, aerospace, manufacturing, energy production and premium consumer goods [1]. PMSM's exhibit numerous advantageous qualities compared to other motor topologies which include, high power density, high efficiency across their range of operation, high starting torque and, high torque to current ratio, wide speed range and constant power operation, high intermittent overload capabilities, reliability and robustness and low acoustic noise and vibration [2]. Due to their favourable qualities compared to other motor topologies, PMSM's are being readily incorporated into numerous different areas in order to help tackle the challenge of the increasing electrification of the worlds many technological sectors traditionally held by fossil fuels.

This is evident in the increasing demand for more electrification in numerous industries such as transportation, hybrid

The associate editor coordinating the review of this manuscript and approving it for publication was Bo Pu.

and electric vehicle drive trains, aerospace, and even military applications. This demand is fueled by the necessity to reduce global emissions and dependency on fossil fuels [3]. The increasing adoption of electric vehicles means that PMSM based automotive drive trains with considerable power ratings are being developed for their reduced weight, cost, increased reliability and ability to exclude additional mechanical devices such as gearboxes or harmonic drives. PMSM topologies are well suited for space and weight limited applications such as those in the automotive and aerospace industries [4].

In terms of aviation, research and industrial projects are currently being carried out to utilise the PMSM topology for aerospace applications, especially civilian air transportation, where emissions account for 12% of the global annual emissions output. The number of passengers is set to double by 2035 to 7.2 billion worldwide [5]. Projects such as More Electric Aircraft (MEA) and Hybrid Electric Aircraft (HEA) are attempting to develop high power, high density, and high efficiency alternative propulsion systems for the aviation industry. Currently the target specific power of an electric motor for aerospace propulsion applications is ≈ 40 kW/kg, current state of the art motors achieve only 5 kW/kg [2]. However, a recent advancement in PMSM based electric motors for aviation and other industries has been developed by H3X in the United States. Their PMSM motor achieves a continuous output of 12 kW/kg, weighing only 16 kg with an output of 200 kW [6].

One other area of concern is the efficiency of electrical machines and their contribution to the global consumption of electrical energy. With climate change and an ever-increasing global consumption and demand for electrical energy, it is becoming ever imperative to continue to improve upon electrical motor efficiency in a broader sense, both domestically and industrially. As of 2009 and onwards, the European Commission Regulation (EC) No 640/2009 has shown that continuous incremental improvements to the efficiency of electrical machines has contributed effectively and meaningfully to low carbon economy targets, such as those set by the European Union.

The European eco-design requirements regulation has been extended in scope and was updated on the 1st of July 2021, with a broader scope to include single speed 50 Hz/60 Hz induction machines. The regulation also includes variable speed drives and requires all variable speed drives to reach at least IE level 2 efficiency. Three phase motors with rated power between 0.75 kW and 200 kW must also meet IE level 4 by July 2023. The IE standard is defined by the ratios of the mechanical output power to the electrical input power and includes other machine characteristics in its definition. The EU is the first place in the world to make IE level 4 mandatory for some electrical motors.

IE is a measure of efficiency where, IE1 = standard efficiency, IE2 = high efficiency, IE3 = premium efficiency and IE4 = super premium efficiency. In global terms, it is postulated that electrical motors contribute to around 50% of the world's total electrical energy consumption, making the continued improvement of electrical machines a necessity in combating one of this century's greatest challenges. (Commission Regulation (EU) 2021/341) [7].

II. BACKGROUND

The stator windings of a PM synchronous motor often account for the largest proportion of the total machine losses observed [8], [9], [10]. The losses that can be attributed to the stator windings are defined by two components, DC and AC power loss. The presence of both DC and AC loss effects complicates winding design. Whilst DC power loss components and thermal dependence are well understood in the estimation of machine performance, AC loss components are difficult to compute accurately consuming much computational effort and time. Sufficiently high AC fundamental operational frequencies ($>$ 1 kHz [11]) can have a significant impact on the behaviour of the device due to the presence of eddy currents developed [12].

Both AC and DC effects are a direct consequence of the geometric configuration of the conductors in the winding. The placement of conductors within the slot is of greater importance for minimising AC loss effects as individual conductor geometry, lay in slot and positioning directly affect the AC loss behaviour [13]. Machine designers traditionally would only consider DC losses in the design process due the complex nature of investigating high frequency AC loss mechanisms. Whilst fill factor has been universally seen as an umbrella metric for low loss winding performance, high device operational frequencies mean that AC effects scale proportionally, complicating the winding design philosophy as AC losses become ever more dominant and the need to pay attention to the individual conductors profiles, positioning and lay in stator slot become increasingly important in a windings design [14].

III. SOLUTIONS IN LITERATURE

A technology that is of particular interest is additive manufacturing (AM). Additive manufacturing offers the ability to create unconstrainted three-dimensional geometries which would be unfeasible via traditional manufacturing processes. AM offers the ability to print in a wide variety of materials including, plastics, ceramics, metal alloys and even biological material. AM's ability to offer rapid prototyping and minimal to no material waste makes the technology highly attractive. As of 2018 the additive manufacturing industry (including, hardware, software, materials, production and includes industries such as aerospace, health care and automotive) was worth approximately \$9.3 billion. The AM industry is expected to be worth \$41.1 billion by 2027 [14].

There are many companies now incorporating additive manufacturing into both rapid production and high-volume production manufacturing pipelines for aerospace and automotive, such companies include BMW and Airbus [14], [15]. Additive manufacturing has been recognised as a key enabling technology for many industries and coupled with

high precision and high-fidelity electromagnetic simulation models, the technology offers opportunities in many aspects of motor topology design, including windings. Winding designs that would be considered too challenging, costly or simply not possible to produce using conventional manufacturing processes are now potentially feasible using the technology [14], [16].

In this work a concentrated algorithmically generated winding of a PMSM open slot machine has been manufactured using the powder bed fusion process in AlSi10Mg, taking full advantage of the design freedoms offered by the additive manufacturing process. The algorithmically generated winding offers potential efficiency gains and weight savings when compared to traditional wound copper wire windings. The algorithmically generated winding will be tested against a Motorette sub-assembly at a simulated operational temperature and the losses observed will be compared. The manufactured active sections of the winding will then be tested for material properties such as resistivity and electrical conductivity.

IV. PROBLEM DEFINITION

The winding that was simulated and constructed in this work was derived and generated via a combined sensitivity analysis, meta-modelling and genetic algorithm based automated optimisation process. Genetic algorithms have been utilised significantly within literature to design motor parameters and topologies and are stochastic based search methods that take inspiration from biological processes, for example, evolution and survival of the fittest [17]. Target objective functions like maximum efficiency and minimum losses are common metrics when assessing machine performance [18], and were used here to identify superior winding arrangements. Parametric design and optimization are increasingly popular in industry and academia due to improvements in computation power [19]. Key winding attributes such as winding height, length, end winding length and pitch are performed [20], [21].

In this work innovative winding geometries optimised on a per conductor level are considered. This is enabled by additive manufacturing, allowing winding arrangements not possible using traditional drawn copper manufacturing capabilities [16], [22], [23]. The process yielded 46 winding arrangements whose efficiency was superior compared to a benchmark winding configuration. The winding arrangements were identified by the simulation number that they were assigned. Hence forth in this work, all windings will be referred to as "#" followed by a number, for example, #7777. Two of the most performant winding designs identified were windings #9354 and #8032, which are shown in Figure1.

Both windings represent cross-sectional arrangements of a concentrated winding design. They were simulated within a permanent magnet machine topology. Designs were simulated firstly in two-dimensional Motor-CAD and Maxwell simulations followed by a three-dimensional high precision Maxwell simulation with a coupled thermal analysis being utilized to confirm simulation precision and accuracy. An open stator slot topology was chosen because it is favorable in the use of prefabricated and preprocessed windings [24]. The PMSM topology and machine parameters are shown in Figure 2 and Table 1.

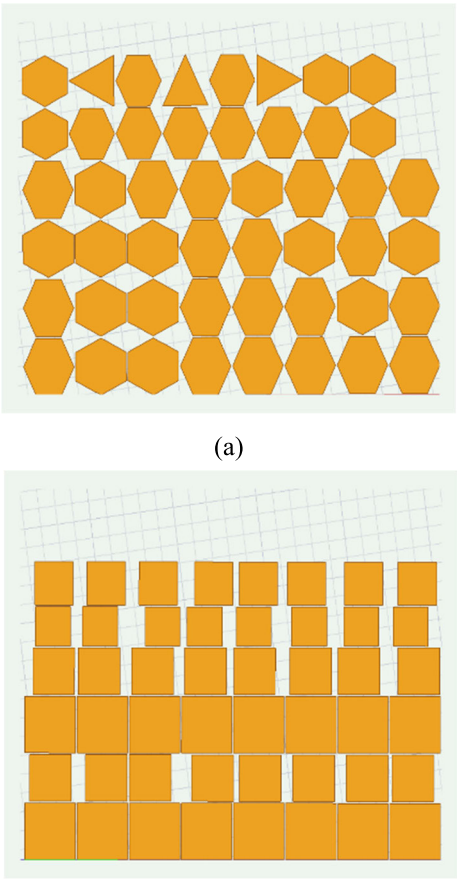

(a)

(b)

FIGURE 1. Winding design #9354 (a) and winding design #8032 (b).

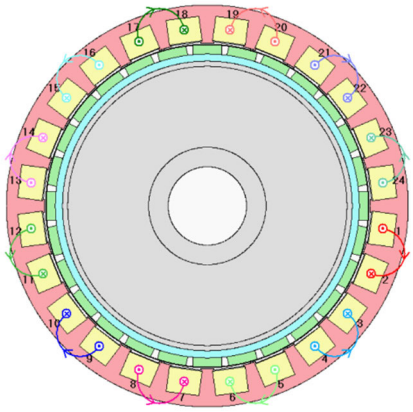

FIGURE 2. The PMSM topology.

Both designs were rendered into high precision three dimensional models utilised in the three-dimensional high

TABLE 1. PMSM machine parameters.

	Concentrated winding machine
Phases	3
Winding throw	1
Parallel branches	4
Winding layers	1
No of conductors per slot	48
Slot number	24
Pole number	28
Stator diameter (mm)	208
Stator length (mm)	210
Motor length (mm)	340
Slot width (mm)	25
Slot height (mm)	20
Tooth tip height (mm)	1
Machine speed (RPM)	1500

precision simulations. Figure 3 shows the 3D model of winding design #9354.

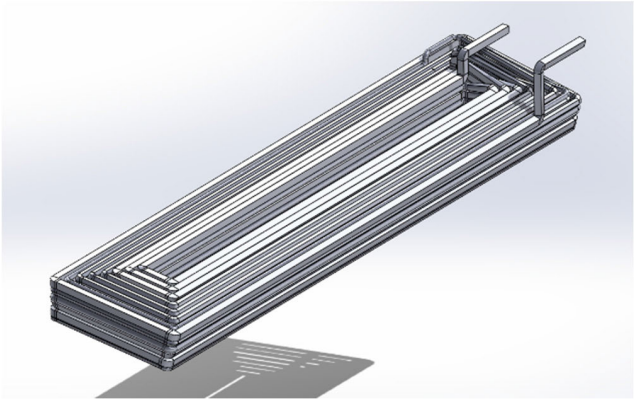

FIGURE 3. Winding design #9354 3D model.

The optimisation process was a fully automated parametric design process, enabled through the use of extensive and numerous custom written Python scripts and API's to connect Ansys Optislang, Ansys Motor-CAD and Ansys Maxwell to form the complete process chain.

Ansys Optislang is a toolbox of algorithms and analytics functionality that can be programmed visually, and that can be automated to carry out a series of optimisation, algorithmic and analytical steps. Whilst Optislang has native connectivity with simulation packages such as Ansys Motor-CAD to a limited degree, a key feature is its ability to extend its functionality via Python scripting. This capability was used to communicate directly with a custom and novel hybrid analytical-finite element analysis model constructed within Ansys Maxwell, enabling the construction of highly complex winding arrangements which are not possible within Ansys Motor-CAD. The optimisation process constructed in Ansys Optislang in shown in Figure 4.

The optimisation process consisted of four conductor placement strategies, orderly placement, layered placement, random placement and clustered placement. The orderly

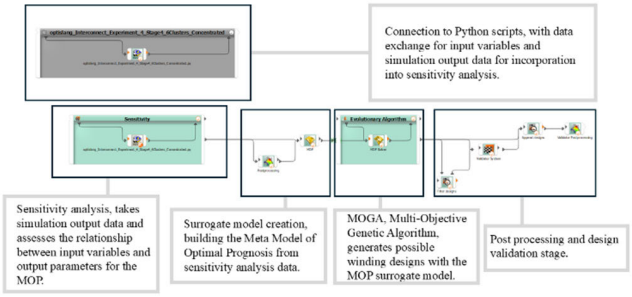

FIGURE 4. The Optislang automated optimisation process workflow.

placement strategy arranged the conductors in an orderly manner, where conductors were equidistant and uniformly placed within the slot. Each conductor had defined and pre-determined area for which they could move, scale, change shape and orient themselves within. The layered placement strategy built upon the orderly strategy, whereby, the slot was divided into sub domains that could grow or shrink in height. The randomised conductor placement strategy utilised an adaptation of the fractal random algorithm by the authors Shier and Bourke [25]. The unique algorithm attempts to solve the random placement of conductors of varying shape, size and orientation within the slot whilst guaranteeing a solvable solution is found. A purely randomised placement is exceptionally time consuming, and solutions are not guaranteed, which is unviable given the large number of simulations needed for sensitivity analysis to take place. Therefore, a fractal randomness is utilised where every n^{th} conductor is slightly smaller than the last. The difference in the conductor scales between every n^{th} conductor is dictated by values of C and N.

$$\mathrm{S(c,\,N)} = \sum_{i=0}^{\infty} 1/(i+N)^{c} \tag{1}$$

The Hurwitz zeta function is an ever-decreasing exponential function, whose values of C and N were pre-computed. Lastly the clustered conductor placement strategy, placed conductors within a volume that could be moved around the available slot space. This arrangement was loosely inspired by bundled conductors. To minimise experiment complexity, solving time and reduce the number of variables being utilised, the conductor shapes were minimised to four base shapes, square, circle, triangle and hexagon. Each experimental placement strategy was run four times, with each starting stage consisting of a seed shape according to the shapes being utilised for conductor profiles. To minimise the number of variables being altered, reduce complexity, provide a better insight into optimisation process and explore the design space thoroughly, experiment runs were separated into stages, with each stage representing one of the degrees of freedom, such as conductor position, size, shape or orientation. The end product of the optimisation step was then used as a seed for the next stage. Figure 5 shows an example of how the winding design evolved per stage, for both concentrated and

distributed windings. Figure 6 shows example winding outputs from the winding optimisation process.

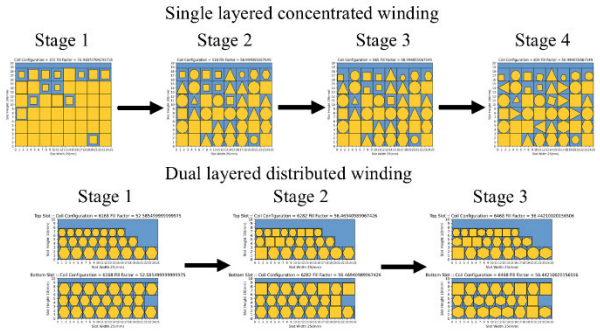

FIGURE 5. The optimization process, per stage outcome examples.

In total there were 248 variables describing each windings layout, regardless of placement strategy. Variable data describing each of the windings 48 conductors was passed directly to the custom Python scripts, which generated a per winding unique visual basic descriptor file, containing thousands of command lines used to draw and place conductors, parameterise and setup a per winding custom PMSM model within a novel hybrid analytical-FEA electromagnetic model used for the optimisation process. The hybrid analytical-FEA model was developed with the CEFEA concept in mind. Computationally Efficient Finite Element Analysis (CEFEA) exploits existing electrical symmetry and magnetic periodicity of PMSM motors with sinusoidal excitation. By designing with CEFEA in mind it is possible to reduce computational time by up to two orders of magnitude [26]. CEFEA was achieved by using model symmetry but by also using analytical assumptions for most of the windings except for one fully composed high precision winding consisting of exacting conductor geometry, placed autonomously by the visual basic descriptor file.

The large, coloured squares represent the analytically represented windings whose properties are computed via analytical assumptions, for example, 100% fill factor, constant conductor height and shape etc, whilst the fully composed winding uses FEA to compute the exact losses produced by a particular design. This was possible as both the analytical and FEA windings were excited via currents, therefore with the windings having the exact same number of turns (48) for both analytical and FEA windings, the EMF and MMF are identical, leading to the machine producing known torque and power values established with the benchmark winding in illustrated Figure 8. The only property that differentiates the analytical and fully composed windings is the loss data, which, for final loss measurements, the loss data for the FEA winding is superimposed across all windings within the machine to give the final loss output. This approach was validated against an identical benchmark winding that was analysed both within Ansys Motor-CAD and replicated exactingly within the Ansys Maxwell Hybrid model detailed in Figure 7.

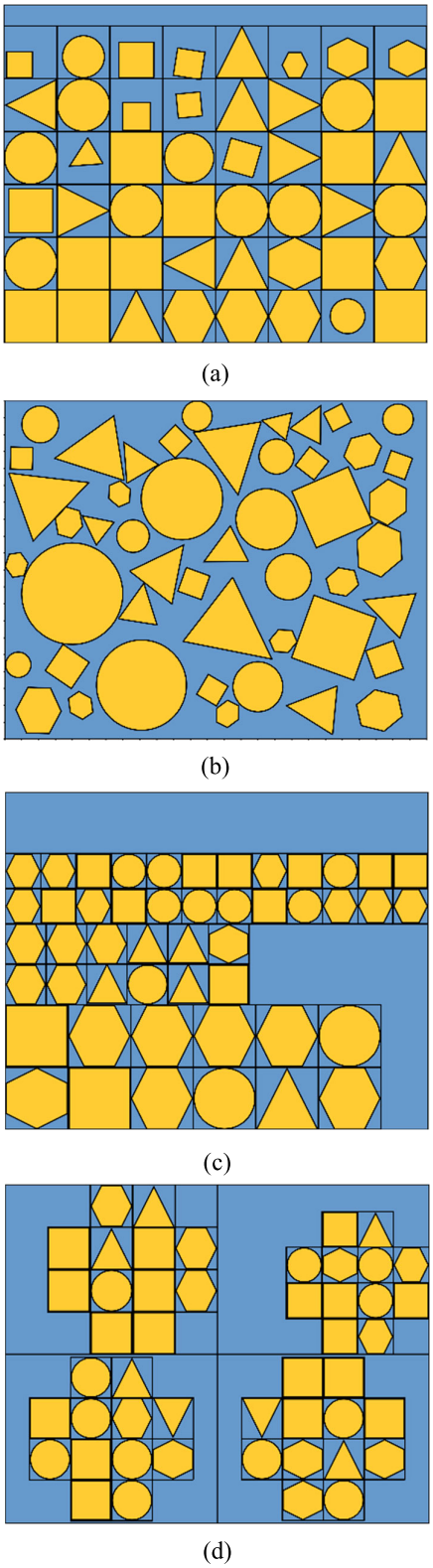

FIGURE 6. Orderly placement (a), random placement (b), layered placement (c) and clustered placement (d).

The hybrid PMSM model was specifically developed to reduce computation time, with the model completing simulations within approximately ∼2 minutes. To further simplify

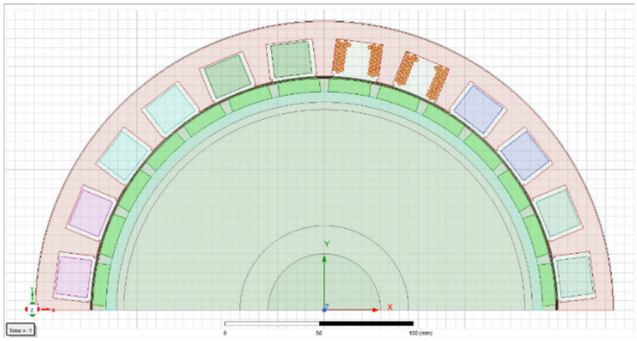

FIGURE 7. The hybrid-analytical-FEA electromagnetic model.

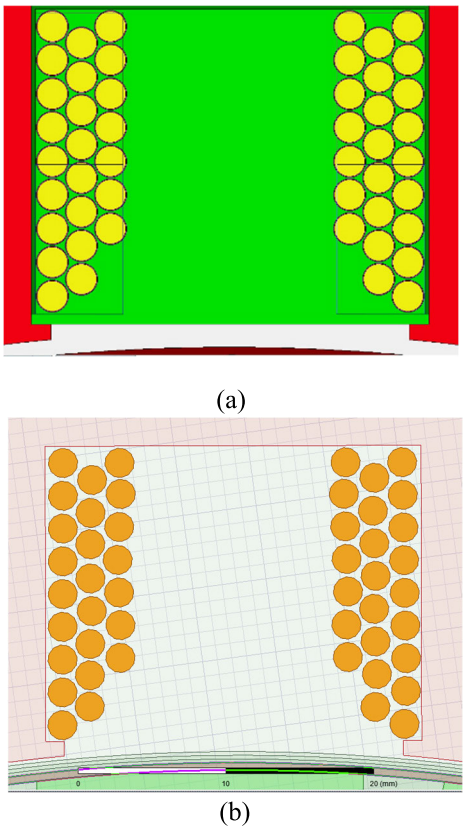

(a)

(b)

FIGURE 8. The benchmark winding in Motor-CAD (a), and the benchmark winding replicated in Ansys Maxwell (b).

the model, lumped parameter thermal networks (LPTN) were used to define the model behaviour at set operational temperatures. Lumped parameter thermal networks are widely used in the thermal analysis of electrical machines and can be preferential due to their reduced computational times [27]. LPTN's are used to reduce model complexity and use heat transfer theory to make estimations about the thermal behaviour of the systems they represent [28], [29]. An example of an LPTN developed in Ansys Motor-CAD is shown in Figure 9.

The LPTN's were created within Ansys Motor-CAD utilising the benchmark winding layout in Figure 8. An individual

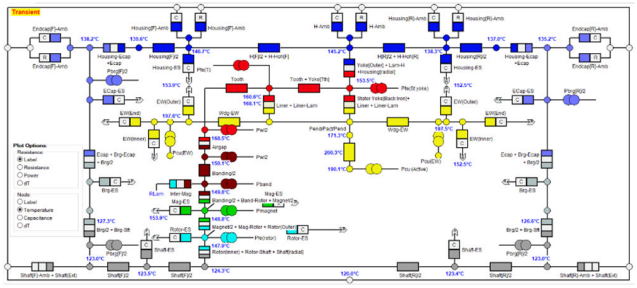

FIGURE 9. The LPTN's created within Motor-CAD.

LPTN was created for both concentrated and distributed winding types. The hybrid model is used specifically in the sensitivity analysis stage in Figure 4 of the optimisation process within Optislang. Sensitivity analysis is the study of how the output of a model can be evaluated, either qualitatively or quantitatively with regard to varying sources of input. Sensitivity analysis is used to quantify the contribution of an optimisation variable to the potential improvement of a model's response. It quantifies the contribution with respect to defined variable ranges [30]. Typically, sensitivity analysis requires large amounts of data, computation and simulation effort, hence why the hybrid analytical-FEA PMSM winding model had to be as computationally efficient as possible. The next stage in the optimisation process is the building of the surrogate model, or in this case the Meta-model of optimal prognosis (MOP). The MOP is a mathematical surrogate model of the various winding arrangements simulated with the hybrid analytical-FEA PMSM model. The MOP maps the complex relationships between the various input and output variables and the relationships that comprise them. The MOP is capable of representing complex models such as the hybrid analytical-FEA PMSM winding model and improves the optimisation execution time, especially with large parameter sets and complex functional relationships. Whilst the combination of meta-modelling and sensitivity analysis is still computationally intensive, involving large data sets, in this case, ∼300-500 samples/simulations per experiment stage, it allows the surrogate model to be improved by removing unimportant variables and reducing variable ranges within the model. This is important as the predictive quality of the MOP and a surrogate model increases as the number of variables decreases [31]. The purpose of meta-modelling is to allow for the rapid evaluation of design trade-offs and is a common tactic used in motor design [32]. Figure 10 shows the accuracy comparison between the MOP and the FEA model it represents.

Finally, the Multi Objective Genetic Algorithm (MOGA) uses the surrogate model to iterate upon possible winding designs based on the objective functions of minimal motor losses and maximal motor efficiency. Genetic algorithms are an example stochastic optimisation [33], [34], in which random search of the optimisation space is used as opposed to deterministic methods that are linear search methods.

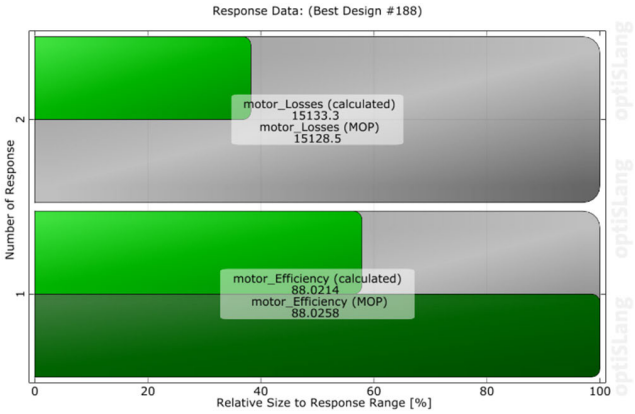

FIGURE 10. An example response data, comparing the accuracy of the MOP against actual simulation values of the objective functions, verifying the accuracy of the surrogate model.

Stochastic search methods offer advantages over deterministic methods such as being more time and compute efficient compared to stochastic methods but also are less likely to get trapped in local optima, whilst handling large numbers of variables and parameters. Stochastic methods are gradient free and possess a continuously evolving population of potential solution candidates. Stochastic methods such as genetic algorithms have been shown to be advantageous in engineering optimisation scenarios and have a distinct advantage with multi-physics problems [1], [35], [36], [37].

The MOGA input parameters were defined as the variables that were of interest and their respective ranges. This varied per experiment basis and many parameters were constrained based on physical attributes such as conductor height, the availability of slot space to move within, the capability to be rotated etc. The objective functions were to maximise overall motor efficiency and minimise overall motor losses, constrained to just the winding geometry and placement within the available slot space, no further topology changes were made. End design ranking was done via pareto front. For the genetic algorithm parameters, the parameters applied were based on experimentation to assess both accuracy of the results and the most optimal use of compute and time resources. Due to the number of variables, 48 per experiment stage, the population size was 150 with the number of generations being 200 to allow the algorithm to explore the search space effectively. The crossover rate was 0.9 to promote high exchange of genetic material parameters between solutions. Mutation rate was 90% to introduce enough diversity to help the algorithm overcome local optima solutions. Selection was done via pareto front for optimal solutions with tournament selection size of 4, to ensure that premature convergence was avoided. Stopping criteria was 20 generations with a minimum change in solution of 10%. This helps the algorithm avoid further optimisation results that may yield diminishing returns.

All windings were optimised for a singular operational point of 1500 RPM and with an open slot topology which is favourable to pre-fabricated and pre-processed windings such as those manufactured by additive manufacturing [24]. The single operational point meant that windings were relatively efficient up until the operating speed of 1500 RPM, after which, winding efficiency would decrease, and losses would increase substantially. This is due to the dominant form of loss being DC loss with proximity losses being the dominant form of AC loss which scaled according to operational frequency. This behaviour is illustrated in Figure 12. Windings would also attempt to avoid armature reaction caused by leakage flux being funneled into the slot by the open slot configuration, this resulted in many different windings placing smaller conductors at the top of the slot to avoid this situation in an attempt to minimise losses due to proximity effects. Larger conductors were placed at the bottom of the slot to help aid fill factor and offset DC losses effects such as I^2R but also help in maximising surface area by minimising current densities associated with the short circuiting of the magnetic circuit of those conductors closest to the back iron. Square conductors are prominent in a number of designs, due to their large copper surface area, compact winding structure and space saving capabilities. Square conductors have also been shown to have superior electrical and thermal performance at lower frequencies [38]. Alternative examples of windings produced by the optimisation process are seen in Figure 11, where the top winding designs are concentrated windings and the bottom winding designs are dual layered distributed winding examples. An example of winding loss densities is shown in Figure 13.

A more comprehensive and detailed description of the hybrid model, optimisation strategy, the processes involved, and the outcomes have been detailed in McKay et al. [39].

However, challenges were encountered when attempting to manufacture the winding configuration as constructed for simulation, illustrated in Figure 3. The additive process chosen to manufacture the part was the laser bed powder fusion process (L-BPF), as it is the most prevalent and commonly used, utilising a wide array of materials. The default material chosen to render the winding was CuCp, a material closely resembling the material properties of pure copper. Numerous external manufacturers cited the complexity in removing internal supports and the close proximity of conductor geometry. This is a common challenge seen in literature and can be considered a current key factor in limiting more complex geometry and thus design freedom [40]. Another concern when utilising additive processes such as L-BPF, is coppers ability to readily absorb and reflect laser source energy, oxidation and unstable melt pools [41], [42], [43], [44].

Besides the difficulties in conductor proximity and the removal of support structures between conductors, another challenging area was the end winding sections. As can be seen in Figures 7, 12 and 13, the windings were mirrored. This was a twofold approach, firstly to further simplify the optimisation process by only optimising one slot of conductors instead of both. This helped scale back simulation complexity

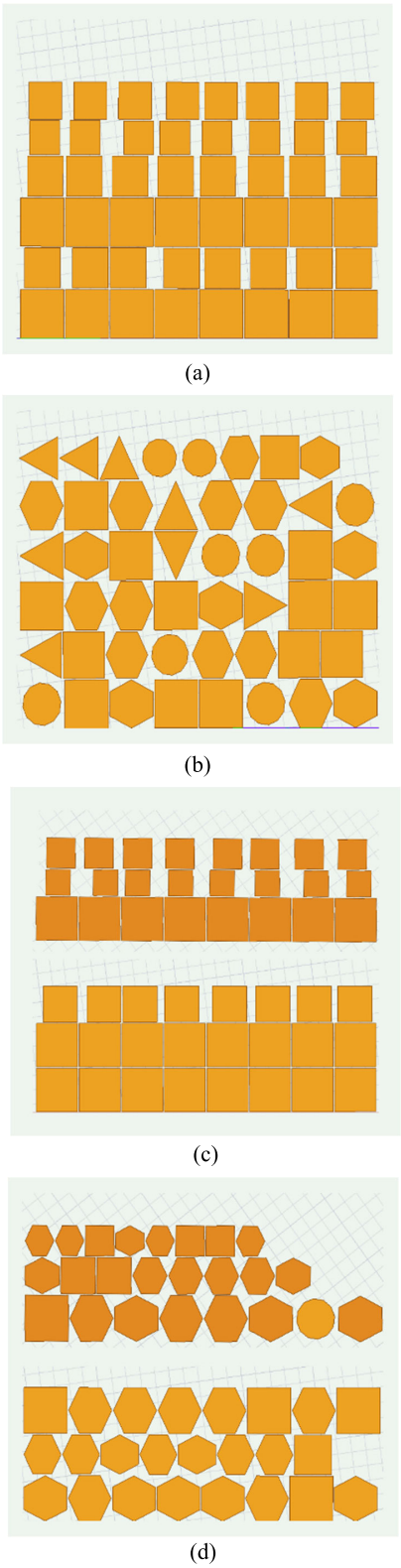

FIGURE 11. Winding #5347 (a), winding #8937 (b), winding #5347 (c) and winding #6468 (d).

and saved on computation time. The second benefit to this approach was to simplify end winding sections, illustrated in Figure 14.

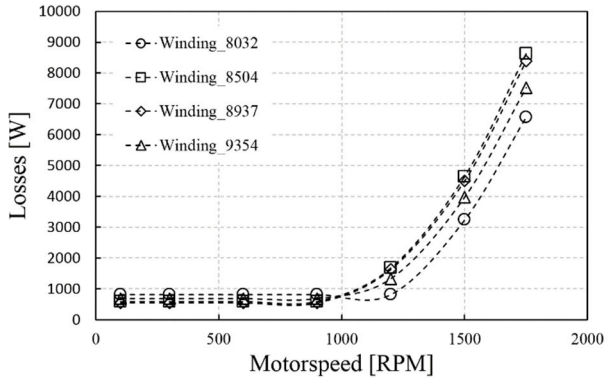

FIGURE 12. An example of the winding behaviour over the operational speed of the PM synchronous motor, from 0 to 1750 Rpm.

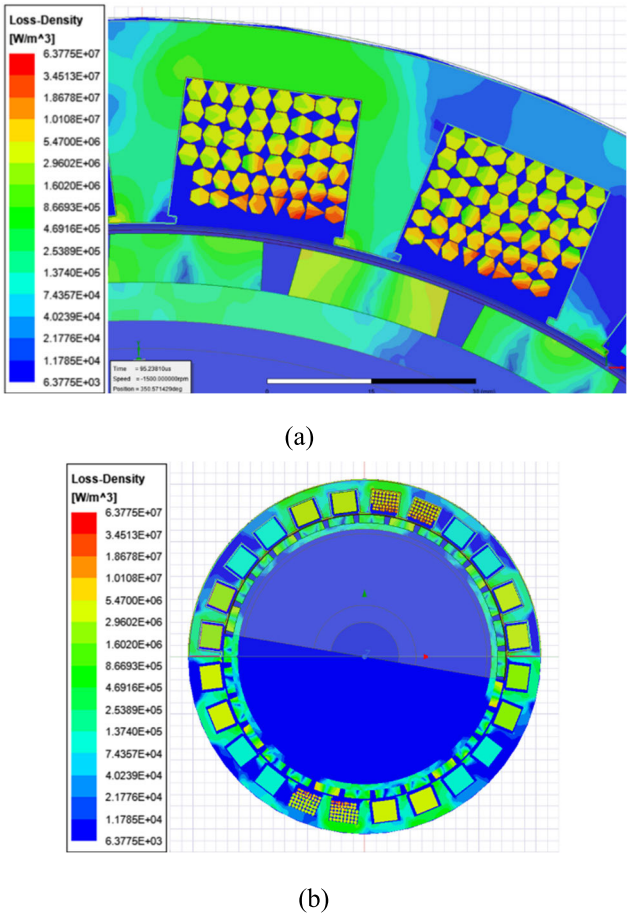

FIGURE 13. An example of the winding loss densities in winding design #9354 (a) and an example of the CEFEA concept (b).

As can be seen in Figure 15 all windings had a standard winding topology, which minimises end winding lengths to those simulated for within Ansys Motor-CAD and the Ansys Maxwell Hybrid PMSM model and 3D high precision model. End windings were highly compact, in an effort to minimise DC losses and material usage. Short end windings are also especially important for electric and hybrid vehicle applications where there are strict packaging requirements [45].

However, this meant that end windings were complex on one of the sides in an effort to form the winding turns and changes from one conductor shape to another.

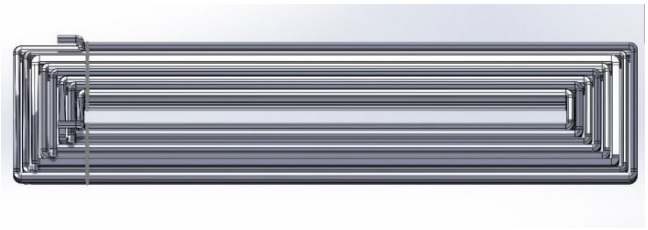

FIGURE 14. Concentrated winding topology.

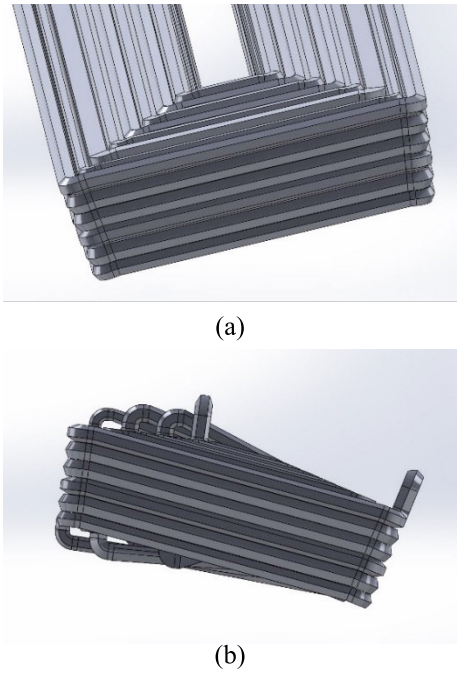

(a)

(b)

FIGURE 15. An example of the opposing end windings, (a) is the standard uniform end winding turns and (b) is the complex end winding turns.

Figures 15 and 16 shows the complex conductor end winding pathways that were formed to facilitate the turns. These end winding structures were a significant challenge as their proximity to one another posed a similar concern for removing support structures. The complex shapes and small cross-sectional area's from 1 mm^2 to 3 mm^2 posed significant challenges due to overhanging sections, feature reproducibility and sheer geometry complexity. Whilst it may have potentially been possible to split the end winding sections from the active sections and attempt to manufacture them separately, the sheer number of potential batches needed and potential number of manufacturing attempts required, would bloat the manufacturing time and cost significantly. Whilst CuCp was the original conductor material, AlSi10Mg was chosen as an alternative as it has been utilised in similar additively manufactured winding scenarios [46], [47].

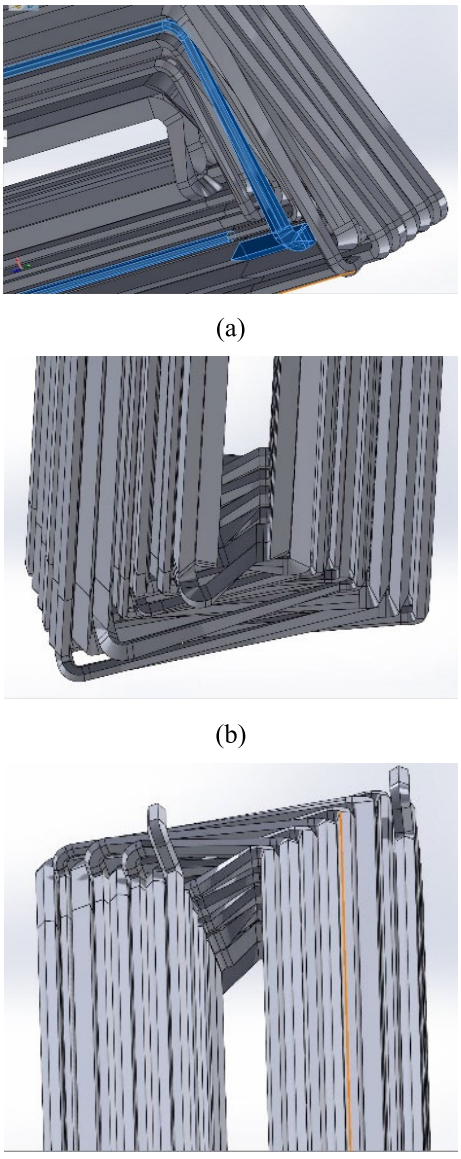

(a)

(b)

(c)

FIGURE 16. Different viewpoints (a, b, c) of the complex end winding arrangement at the connection side.

In light of these concerns, two changes were made when manufacturing the winding geometry:, i) the winding material was changed from CuCp to AlSi10Mg, and ii) only active section geometry was manufactured. AlSi10Mg was selected due to its ability to manufacture intricate fine features compared to copper, it is also utilised in industries such as aerospace and has been used previously to manufacture winding geometry using L-PBF [18], [20], [48], [49], [50]. Both winding designs #9354 and #8032 active sections were assessed for their fitness for manufacture before delegating to an external manufacturer. The geometry to be printed was simulated in Simufact Additive. It was found that the most performant winding #8032 developed excessive deformation during the simulation process leading to build failure, shown

in Figure 17. Winding #9354 however, successfully completed the simulated build process with minimal geometric deformations, as shown in Figure 18.

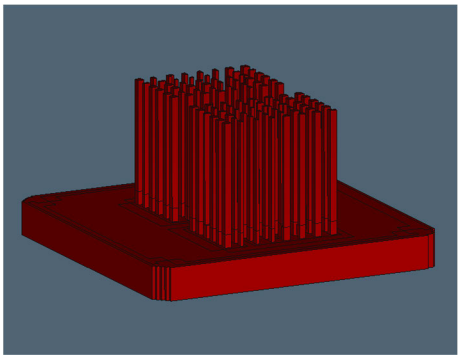

FIGURE 17. Winding design #8032, showing Simufact Additive build failure due to excessive deformation.

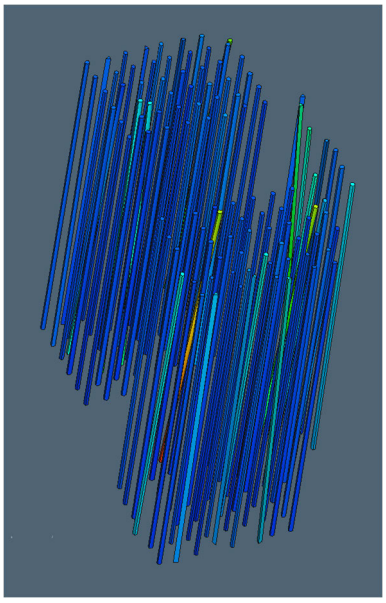

FIGURE 18. A successful Simufact Additive simulation of winding design #9354 build process, showing slight deformation.

The active sections were printed in the vertical orientation as this allowed all the sections to be printed in one pass, ensuring homogeneity and minimising space usage in the build area, which allows for minimal support structures and has been shown previously to improve the electrical properties of the parts. This is due to the presence of aluminium rich connected areas, where electrons can pass more freely, minimising their interaction with aluminium silicon boundaries and silicon rich formations [51], [52]. Before issuing the build to an external manufacturer, the build was first tested at an internal facility ''NMIS Boeing'' to troubleshoot for potential unforeseen build challenges. The sections were rendered in Steel 316L using the Renishaw AM 500 shown in Figure 19.

Once confident the active sections could be printed reliably, an external manufacturer capable of printing AlSi10Mg

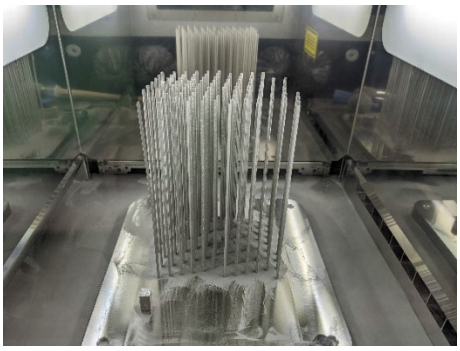

FIGURE 19. Winding design #9354 active sections rendered in Steel 316L using the Renishaw AM 500.

parts was assigned with the build. The active sections for winding #9354 were rendered using the SLM 280 by SLM. Table 2 shows the SLM machine parameters.

TABLE 2. The SLM 280 machine parameters.

Build area (L x W x H)	280 x 280 x 365 mm
Laser configuration (3D Optics)	Single 400W IPG Fiber Laser
Real Build Rate	113 cm^3/h
Layer Thickness	90 µm
Minimum Feature size	150 µm
Beam Focus Diameter	80 – 115 µm
Maximum Scan Speed	10 m/s
Average Inert Gas Consumption in Process	5 L/min (Argon)
Average Inert Gas Consumption in Purging	110 L/min (Argon)
E-Connection / Power Input	400 volt 3NPE, 63 A, 50/60Hz, 3.5-5.5 KW
Compressed Air Requirement	ISO 8573-4:2010 [1:4:1] 7 bar
Machine Dimensions (L x W x H)	2600 x 1200 x 2700 mm

The powder feedstock and AlSi10Mg specifications as supplied by the manufacturer are shown in Table 3.

TABLE 3. The powder feedstock chemical composition.

chemistry	Si	Mg	Mn	Al	Fe	Cu	Zn	Sn	Pb	Ti	Ni
Minimum	9.0	0.20	-	-	-	0.10	-	-	-	-	-
Maximum	11.0	0.45	0.45	-	0.55	<0.01	0.1	0.05	0.05	0.15	0.05
Result	9.73	0.33	<0.01	90.0	0.078	0.010	0.010	<0.01	<0.01	<0.01	<0.01

Particle size as indicated by the supplier was 20-63 μm.

Winding active sections were manufactured as-is and surfaces were not polished or treated in any way to ensure conductor geometry remained intact, as surface polishing would remove conductor corners and details. The end windings were constructed from 14 AWG, multi-strand copper wire with custom made, pure copper sheet-metal connectors to minimise contact resistance. Every turn had a pre-defined length to make calculation of theoretical winding resistance easier. End winding contacts also allowed for the fine tuning of conductor rotation and placement within the slot. End windings are shown in Figure 20.

The contacts were insulated using Polyimide high temperature resistant electrical tape. Polyimide is capable of withstanding temperatures of up to 260°C and has a high dielectric strength of 7000 V [53]. In the original winding design in Figure 3, the end windings were 2.5 cm in length with the active sections being 21 cm long. The winding constructed for the experiment comprises of 21 cm active

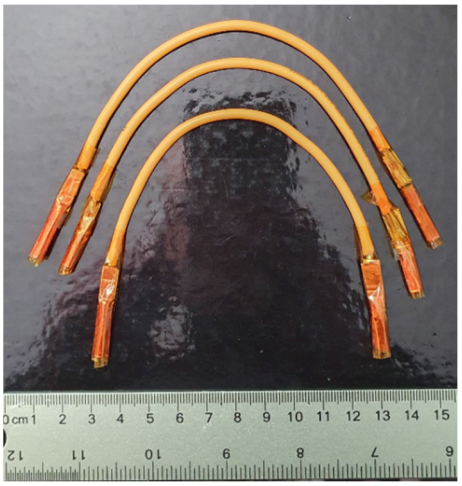

FIGURE 20. The end windings.

sections with an additional 2 cm either side to allow connection of end windings. Compared to the original winding design, the constructed winding measured 37 cm in length in total, with the copper end windings comprising the additional 6 cm of end winding length. The original simulated winding is 25 cm in length. Active sections were insulated using Polyimide electrical tape.

In terms of the stator material, the original stator material was M350-50A, but due to challenges in acquiring M350-50A, the stator laminations were therefore changed from M350-50A to M270-50A. The number of stator laminations were therefore increased from 410 laminations to 600 laminations. The stator was manufactured and constructed by Tannlin UK Ltd. Slot insulation material is comprised of VonRoll. Figure 21 shows the completed experimental Motorette sub-assembly.

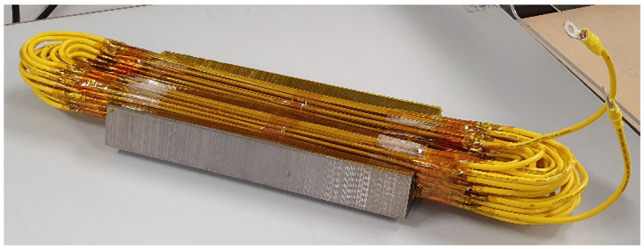

FIGURE 21. The final constructed experimental winding #9354.

V. EXPERIMENT AND RESULTS

The experiment comprised of two parts. Firstly, a measurement of RDC and RAC was taken and a value of RAC/RDC was identified. Secondly, measurements were taken for resistivity and conductivity for a selection of conductor lengths of different shapes and compared against previously established values. The measurement of RDC involved a DC winding test, injecting a 10A DC current into the winding and measuring the voltage and current drop across the winding. An RS PRO RS-12T TRMS Auto-ranging Digital Multimeter was used to measure both sets of values. The RAC measurement similarly involved injecting an AC 350 Hz 0 phase angle signal at 10A RMS into the winding and measuring the RMS values of current and voltage dropped across the winding.

A single-phase 350 Hz inverter was constructed utilizing the FX278379D signal processor to generate a sinusoidal pulse width modulated signal driving four gate drivers. The gate drivers provide the necessary gate voltage to switch the IGBT bridge circuit. IGBTs used were the Infineon AIGW40N65H5XKSA1. Three k-type thermocouples and temperature measurement devices were attached to the winding, stator and end windings to monitor temperature fluctuations. The experiment was run at was room temperature. The experimental setup is shown in Figure 22.

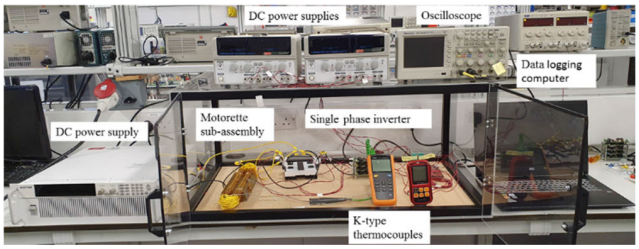

FIGURE 22. The practical experiment setup.

A new set of two dimensional and three-dimensional high precision models were produced to account for change in materials. It is these simulated loss models that the experimental test data were compared against. The windings room temperature resistance was taken via the BK Precision 2840 DC Resistance Meter, shown in Figure 23.

FIGURE 23. The BK Precision 2840 DC Resistance Meter.

The losses produced by the experimental winding are substantial, which is due to the larger winding resistance compared to the theoretical and simulated winding resistances (Table 4). Compared to the theoretical hybrid winding, the measured resistance is twice the size of the exact same winding with calculated resistance. The theoretical hybrid winding assumes perfect connections between the active sections and the copper end windings, whilst in reality these connections

TABLE 4. The experimental and simulation results.

	Winding Resistance (Ω) @ 20 C	DC power loss (W)	AC power loss (W)	RAC/ RDC	Total power loss (W)
AlSi10Mg simulated Winding	0.186	669.332	1122.003	1.676	1791.335
Experiment winding	0.441	1587.503	2425.939	1.527	4013.441
Hybrid winding (AlSi10Mg + Copper end windings)	0.211	759.457	1273.079	1.676	2032.536
AlSi10Mg simulated winding with Measured RAC/RDC	0.186	669.332	1022.144	1.527	1691.477

are imperfect, however the experiment windings resistance is still considered within an acceptable range for a three-phase winding of ≈ 0.3 to 2 Ω [54].

Using the theoretical hybrid windings resistance and simulated RAC/RDC the total power loss is close to the simulated value of power for the simulated AlSi10Mg winding. Utilising the measured RAC/RDC value for the experimental winding with the simulated AlSi10Mg windings resistance, a total power loss of 1691.48 W is achieved compared to the simulated value of 1791.34 W. The values being comparatively close, illustrate a potential for the simulated winding to match the expected total simulated loss if it could be replicated precisely as per the design.

There are several reasons for a mismatch between the measured RAC/RDC and the calculated RAC/RDC. For example, the measured DC resistance is relatively high due to imperfect end winding connections and larger end windings in general. The experiment winding layout was also most likely not perfectly replicated in line with #9354's design leading to additional AC losses. Most importantly, the Motorette model was unable to replicate the armature reaction field generated by the permanent magnet material on the rotor, which would lead to additional proximity effect losses in the open slot configuration of the stator. The difference in simulated losses to those achieved using the measured RAC/RDC of the additively manufactured winding was 9.4%.

Whilst the winding could not be replicated exactly 1:1 with the three dimensional simulated design using the L-BPF manufacturing method, another method such as binder jetting may offer the ability to produce such a structure, due to the ability to produce parts without support structures [55]. At the time of doing the research and manufacturing for this work, binder jetting was currently unavailable commercially but may be available at a future date. Therefore, further research in investigating the ability for binder jetting to produce highly complex winding geometries such as those presented in this work, would be recommended.

The second experiment comprised of testing 3 samples of conductor active sections rendered in AlSi10Mg of differing cross-sectional shape and area. A large hexagon, small hexagon and small triangle were tested as these were the cross-sections utilized in winding #9354's layout. The resistance was measured at room temperature using the BK 2840 Precision DC Resistance Meter. Values of resistance are shown in Table 5. Resistance was measured at room temperature using the BK 2840 Precession DC Resistance Meter. Figure 24 shows the measured resistivity, conductivity and IACS%.

TABLE 5. Conductor sample values.

	Resistance (Ω)	Cross sectional area (mm^2)	Length (mm)
Large hexagon conductor	0.001652	6.863	250
Small hexagon conductor	0.001987	5.467	250
Small triangle conductor	0.002653	3.645	250

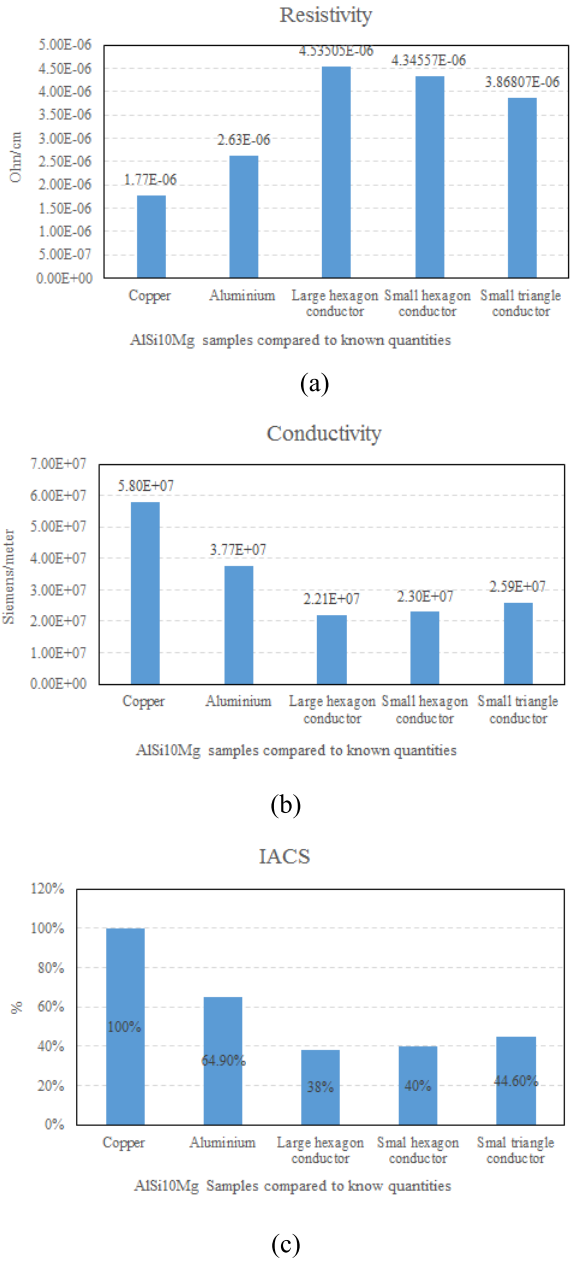

FIGURE 24. The measured resistivity (a), conductivity (b) and the IACS% (c).

The resistivity of all three samples aligned with previously stated ranges for AlSi10Mg within literature [41]. Consequently, the conductivity follows the same trend. The samples

achieved ≈ 41% IACS on average compared to copper (100% IACS) and aluminium which is ≈ 65% IACS. The electrical resistance of a conductive material is due to the variation and disruption of the lattice structure of the material at the atomic scale [51]. Interestingly, the smaller shapes with smaller cross-sectional areas produce slightly lower resistivity and higher conductivity than the larger hexagon shaped conductor. This could be due to a slightly higher density in those parts [40], which will be experimentally verified in future work. This may be due to a more favourable laser cross-hatching pattern being utilised to render those shapes compared to the larger hexagonal conductor, producing a higher density part.

VI. SUSTAINABILITY AND THE SUITABILITY OF ADDITIVE MANUFACTURING

Sustainability has become a major concern for all organisations within the digital and circular economy [56]. Businesses and governments have made commitments to long-term goals such in reducing their environmental impact and resource conservation [57], and a rapidly changing business environment due to sustainability has meant that sustainable manufacturing has become an ever-growing research area [58]. One of the most important questions in terms of sustainability is how to ensure environmental and social protection without compromising economic growth [57].

One such solution is the introduction of the concept of Industry 4.0. Industry 4.0 inspires large organisational changes using the benefits of new technologies which focus on the collaboration between systems such as machine to machine and human to machine interactions. The concept promotes agility, decision making, efficiency, cost reduction and flexibility. Industry 4.0 aims to develop processes and services using technology to help control industrial processes and operate and react in real time [59], [60], [61]. The fourth industrial revolution is the result of the digital revolution where new software, robotics and technologies help to integrate physical and digital systems resulting in fast product development and manufacture. Industry 4.0 offers to increase production turnover and achieve better results [62] and is a change in the manufacturing business model that helps production efficiency, flexibility and productivity through the inclusion of advanced technology and communication channels. It consists of both physical and digital technologies. Digital technologies include computer systems, cloud computing, blockchain, simulation systems, artificial intelligence, digital twins, horizontal and vertical integration and augmented reality. Physical technologies include sensory systems, drones, robotics, global positioning systems, mobile technology, nanotechnology, and novel manufacturing technologies such as additive manufacturing [59], [63]. With greater climate concerns and more stringent environmental regulations, industries need to develop and implement manufacturing solutions that produce less harmful emissions and by-products compared to existing traditional manufacturing processes [64].

Additive manufacturing promotes sustainable manufacturing [65], [66] and helps with the elimination or significant reduction in waste material, achieving sustainability [67]. The implementation of AM is often cited as the future of manufacturing offering numerous benefits to society, as it offers the versatility of reduced machine cost and increased design freedoms for complex geometries garnering interest both academically and industrially [68]. In comparison to traditional subtractive manufacturing processes, AM is claimed to be a green technology with the promise of improved resource efficiency, using less energy, material resources and reducing emissions [69], [70]. Sustainable AM provides more sustainable production opportunities leading to more sustainable business opportunities in reducing energy consumption, CO2 emissions and production costs, whilst positively impacting waste management and operational safety [71].

AM is economically viable for small to medium batch production scenarios [72], [73] and is best suited for low production manufacturing, where high customisability is preferred, with short lead-times and complex geometric capability [74]. It offers the ability for manufacturers to create optimal part designs where lean production is key [74]. However, comparing AM processes to traditional processes is complex and not straightforward.

Production level machines can range from $5,000 to $1,000,000. Additional costs associated with AM include material costs such as polymers, elastomers, metallic powders, resins, wire and sheets. Additional costs include running costs such as electrical energy and inert gas etc [74]. The often-assumed environmental advantages that AM boasts including reduced material waste and better material utilisation are somewhat displaced by their energy consumption which was shown to be 10 - 100 times higher than conventional manufacturing techniques such as casting and machining [75].

Raw material production for AM also requires additional processing steps such as powderisation and atomisation, or wire drawing, dependent on the AM process feedstock material required [76]. Another concern is the quality of AM parts. Poor surface quality and the presence of residual stresses, particularly in metallic parts, may require post-processing, such as finishing machining to achieve the desired surface finish and dimensional accuracy, along with heat treatment to relieve said residual stresses. Lack of product quality leads to consumer dissatisfaction, loss of company reputation, economic losses and wasted resources. Therefore, post-processing cannot be overlooked [77]. Post processing and quality control also incur additional environmental and economic costs associated with them. This construes the advantages such as material savings and can be misleading from a sustainability perspective [76]. The rough surface quality and the residual stresses present within AM parts are a major concern. To achieve the required surface quality, AM parts are subjected to different machine finishing

operations. To relieve residual stresses AM parts are subjected to post manufacturing heat treatment processes. Additional requirements include the removal of support structures and removal of unsintered powder in metal AM processes. These additional processing steps consume additional electricity and generate material waste, reducing resource efficiency and increasing the cost of AM [78], [79].

Metal powders are the most common feedstock material used in many different AM processes such as powder bed fusion (PBF), binder jetting (BJ) and directed energy deposition (DED). They are produced using powder atomisation processes, where a material ingot is melted with the material being disintegrated into fine droplets using a high-pressure stream of gas or water. The embodied energy for the production of AlSi10Mg, the material used in the production of the windings for this work was cited in literature to be 189 MJ/kg [78].

The specific energy for SLM (selective laser melting, terminology often interchangeable with laser bed powder fusion, the AM process used in this work) varies between 55 and 569 MJ/kg. The material waste produced via this process is unsintered powder and supporting structures removed during post-processing. Material wastage can vary depending on the product geometry and orientation. Priarone et al. [78], showed that the additional material required for support structures varied between 30 to 45% of the final part, in 3 different orientations of the same part manufactured using SLM. For the SLM process of AlSi10Mg, the finish machining (post processing) energy consumed was quoted in literature to be around 6.6 MJ/kg [80].

Whilst there appears to be no current information regarding the specific energy for the SLM 280 (the machine used to manufacture the parts in this work) depositing AlSi10Mg as a raw material, the specific energy used for the deposition of AlSi10Mg with the SLM 250, a similarly comparative machine from the same manufacturer is quoted as being 566 MJ/kg for AlSi10Mg [78]. However, for stainless steel, the SLM 280 used a specific energy of 383.13 MJ/kg, with a deposition rate 9.9 cm3/h in literature [81].

The support structures utilised for the SLM 280 range between 4.3% to 34% for stainless steel. For the comparative machine, the SLM 250, the support structures for AlSi10Mg documented in literature are around 30 to 45% of which make up the total material used in comparison to the material comprising final part. 10% was also consumed to post processing machining [78]. Commenting on the structures manufactured for this work using the laser bed powder fusion process, manufactured on the SLM 280 machine, the energy consumed in manufacturing the parts was unknown,. The material waste was kept minimal as the active lengths were manufactured in an upright position. With waste generated from support structures estimated to be less than 5% of the actual material that made up the final parts. However, the amount of powder feedstock material consumed or recycled by the manufacturer is unknown.

LBPF process data on feedstock and the machine being used were ascertained and are displayed in Table 2 and Table 3 respectively. No weight reduction strategies were deployed as the conductors making the winding had to be fully filled and solid for maximal electrical conducting capabilities. A minimisation of conductor volume would lead to an increase in the RDC, since the resistivity and therefore the resistance of a conductor is a function of the area and the length of the conductor.

$$R = \frac{\rho l}{A_{length}} (\Omega) \tag{2}$$

where, ρ is the resistivity of the material, l is the length and A is the cross-sectional area.

If the part was used in a a critical application requiring good surface roughness or appropriate level of tensile strength, post processing such as surface finish or heat treatment would be required to prepare the part for that purpose. In this work no post processing was used to avoid erasure of part surface details, for example, dulling of corners or misshaping the cross sections as to retain as much detail as possible and replicate the winding layout as closely to simulation as possible. This helps aid RDC by retaining cross sectional area, but also helps replicate the complex RAC phenomena and interactions such as skin effect and proximity effect as closely to simulation as possible. Ultimately since no post processing was involved so no additional energy was consumed in.

A common metric for how sustainable an AM process is, is the percentile comparison of waste material to the overall material used to create the part. In the case of the parts produced for the active sections that comprise the winding, small support structures of 1 cm helped to separate the rods from the base plate were used. This aided in cutting the rod like conductor sections from the base plate whilst maintaining their required lengths. It was calculated that the support structures made up just 1.13% of the total volume of the final parts making the orientation and the build strategy deployed highly efficient, however as stated it was unknown how much unsintered material feedstock was consumed and recycled by the manufacturer.

Comparing additive manufacturing to more traditional manufacturing techniques, there have been studies comparing CNC machining against FDM and SLM against casting. Faludi et al. carried out a comparative analysis between FDM (fused deposition modelling) and CNC machining. It was concluded that AM cannot be considered more environmentally friendly than CNC, however, this was dependent upon the manufacturing situation [82].

Vevers et al. [83] compared casting against SLM concluding that whilst the mechanical properties of the parts, such as hardness and tensile strength produced were superior to their casted counterparts, prohibiting factors such as cost and production speed, especially when the parts to be produced numbered into the thousands, was a significant factor in the choice of manufacturing method. Production vol-

ume, part complexity and feature requirements are important considerations. For mass production scenarios casting was considered to be more advantageous, even though the initial costs were significantly higher than that of AM, at around €4000 initially.

Both CNC machining and casting have been explored in literature, to create winding geometry for electric machines. Metal cast windings have been developed by Fraunhofer, illustrating the casting of aluminium and copper windings. However, winding geometry appears to be limited to flat, trapezoidal conductor shapes with low numbers of turns forming the winding. Minimal conductor heights achieved were 0.7 mm with achievable winding lengths of 200 mm demonstrated. Only concentrated windings were created [84], [85].

KITECH, illustrated the manufacturing of high fill factor trapezoidal windings using CNC machining. Once milled the windings were insulated and compressed to fit into the stator slot. However, the processes suitability for mass production is limited and therefore only small batches and prototyping is considered. One such area of deployment could be the aerospace industry where cost and time constrains are less of a limiting factor [85].

To conclude AM, is situation and scenario specific in its deployment, where consideration should be given to how a particular product uses more or less electrical and material resources compared to conventional manufacturing processes. AM is best suited to low production, high value scenarios, small batches, high customisability, short lead times and rapid prototyping [74].

VII. CONCLUSION AND FUTURE WORK

Among the limitations of the work was the experiment set up where the experiment was not carried out with the original 2D and 3D simulations and materials. Difficulty in the manufacturing process and obtaining the original materials resulted in alternative materials being sourced. Therefore, a direct comparison could not be achieved. This challenge was mitigated by producing a new set of 2D and 3D simulations with the new materials, however in future work it would be advantageous to produce a model that perfectly replicated the materials used. Another challenge was the L-BPF process inability to produce the exact winding geometry, however, as stated the binder jetting process may enable the ability to print the entire winding as designed without the need for support structures.

The Motorette sub-assembly could not completely replicate neither the entire range of loss mechanisms, such as armature reaction, nor the original temperature and RMS current values that the PMSM simulated model was computed for. The simulated original machine energised the windings with 62 A RMS per winding with windings running at temperatures of 190°C. Such current and temperature values were deemed too dangerous to be run in a laboratory setting and so DC and AC testing was run at room temperature with 10 A DC and 10 A RMS respectively.

The end winding connections were imperfect and had ramifications for the RDC values obtained for the Motorette winding. The round copper connections connecting the additively manufactured parts to the 14 AWG copper end windings minimised the contact surface area between the active sections and the end windings due to the hexagonal and triangular cross sections being fitted into the cylindrical connections, thereby increasing the resistance. However, it did have the advantage that the position and rotation of the conductors could be finely placed and adjusted within the slot area, which was advantageous while attempting to replicate winding design #9354's layout.

Whilst the Motorette sub-assembly was useful in gauging the viability of the winding, future work would benefit from replicating the entire winding, but also by having an entire PM synchronous motor fitted with additive windings for experimental comparison would be the desired outcome. Having an experiment with two identical PM synchronous motors, one fitted with wound copper windings and the other fitted with all additively manufactured windings would be the definitive experimental setup to identify how additively manufactured windings compare against traditional wound copper windings, in terms of power density, temperature behaviour and loss behaviour. A Motorette sub-assembly cannot replicate the minutia of various loss mechanisms incurred within an actual machine, which is recognised in this work. Another avenue for potential future work would be to study the degradation over time of an additively manufactured winding through temperature cycling and energising and de-energising of the component, especially at the material level.

Optimised winding structures such as those presented within this work could help bring benefits to many different industries and applications. For example, optimised winding structures could help achieve better and optimal drive cycles for traction motors within the automotive industry, especially within battery electric vehicles BEV's and hybrid vehicles where space, weight and cost are defining design features. Drive cycles such as WLTP-3, C-WTVC and NEDC could benefit from windings optimised for a vehicle's specific characteristics, optimising the windings and therefore the electric motors performance over that drive cycle. Operational areas of a motor are dependent on environmental factors such as urban, rural and highway driving. For automotive applications, electric motors are typically designed for the minimisation of material and manufacturing costs, weight, volume and operational loss. [86].

As stated, space and volume are of prime concern with BEV and hybrid electric vehicles, thus optimising winding structure, reducing material usage and minimising winding geometry, especially end-windings and volume, would be key to improving the overall performance of an electrified vehicle [45].

Another area that could benefit greatly from the optimisation of the windings is the aerospace industry where the electrification of aerospace is especially challenging, due to the strict motor parameters outlined by the ASCEND project [86]. The ASCEND projects projected performance metrics are incredibly demanding and stated that the specific power of 20 kW/kg (motor active SP) should be attained, with the motor being able to run high efficiency at continuous operation of 5000 RPM for one minute (take off). This is challenging as there are two unique operational points to be considered, base speed and peak power. This is dichotomous since the RAC/RDC is uniquely different for each operating point, with both AC and DC losses at each operating point being in stark contrast to the other. Complex winding designs such as those explored in this work could help best fit the operational demands for efficiency and power density by helping to minimise design trade-offs for RAC/RDC, which is a well-known engineering challenge.

A more specific example within aerospace is starter motors for traditional and hybridised aircraft, where Fan Wu et al. [46] developed a 250 kW, 20.10 kW/kg permanent magnet synchronous motor achieving efficiency of 96.18%. It was found that a mixture of hollow and solid conductors was the optimal solution to negate armature reaction losses exhibited by the conductors near the top of the slot. The windings were rendered in AlSi10Mg similarly to the windings produced in this work. Whilst the windings were printed and tested via Motorette sub-assembly, the windings were rectangular in shape and not optimal for dealing with more complex loss mechanisms such as skin and proximity effects. Optimisation processes such as those deployed and tested in this work could help further refine and shape the winding to achieve higher efficiency, coolant fluid flow and weight reduction, thereby achieving higher efficiency and power densities for motors required by the electrification of aerospace.

In this work a Motorette sub assembly with a winding in which the active sections were manufactured in AlSi10Mg using the L-BPF method was tested. Samples of the manufactured active sections were measured for resistivity, conductivity and the IACS% compared. It was found that designing a winding to take advantage of the freedoms afforded by additive manufacturing does produce a winding that can closely match the simulated loss profile of an idealized winding geometry. A 9.4% difference in losses utilizing the measured RAC/RDC of the constructed experimental winding was observed, which can be explained through imperfect end winding connections, increased end winding length, non-idealized conductor positioning and the absence of the armature field produced by the permanent magnet material.

REFERENCES

[1] S. Sakunthala, R. Kiranmayi, and P. N. Mandadi, "A study on industrial motor drives: Comparison and applications of PMSM and BLDC motor drives," in *Proc. Int. Conf. Energy, Commun., Data Anal. Soft Comput. (ICECDS)*, Aug. 2017, pp. 537–540.

[2] B. A. Adu-Gyamfi and C. Good, "Electric aviation: A review of concepts and enabling technologies," *Transp. Eng.*, vol. 9, Sep. 2022, Art. no. 100134.

[3] A. Loganayaki and R. B. Kumar, "Permanent magnet synchronous motor for electric vehicle applications," in *Proc. 5th Int. Conf. Adv. Comput. Commun. Syst. (ICACCS)*, Mar. 2019, pp. 1064–1069.

[4] P. Giangrane, V. Madonna, S. Nuzzo, and M. Galea, "Moving towar a reliability-orientated design approach of low-voltage electrical machines by including insulation thermal aging considerations," *IEEE Trans. Transport. Electrific.*, vol. 6, no. 1, pp. 16–27, Feb. 2020.

[5] A. D. Anderson, N. J. Renner, Y. Wang, S. Agrawal, S. Sirimanna, D. Lee, A. Banerjee, K. Haran, M. J. Starr, and J. L. Felder, "System weight comparison of electric machine topologies for electric aircraft propulsion," in *Proc. AIAA/IEEE Electr. Aircr. Technol. Symp. (EATS)*, Jul. 2018, pp. 1–16.

[6] *Integrated Motor Drives for Electric Aircraft, Aerospace, Electric Boats, E-Motorsports, Power Generation and Military and Defence*, H3X Technologies Inc., Denver, CO, USA, 2023.

[7] *Commission Regulation (EU) 2021/341*, The official Journal of the European Union, The European Commission, Strasbourg, France, 2021.

[8] A. Soualmi, F. Dubas, D. Depernet, A. Randia, and C. Espanet, "Study of copper losses in the stator windings and PM eddy-current losses for PM synchronous machines taking into account influence of PWM harmonics," in *Proc. 15th Int. Conf. Elect. Mach. Syst. (ICEMS)*, Oct. 2012, pp. 1–5.

[9] S. Ayat, R. Wrobel, J. Goss, and D. Drury, "Experiment informed methodology for thermal design of PM machines," in *Proc. 11th Int. Conf. Ecol. Vehicles Renew. Energies (EVER)*, Apr. 2016, pp. 1–7.

[10] J. Pecotich, D. Klink, G. Heins, and B. Bahrani, "Additively manufactured electric machine conductors with integrated end turn heat exchangers," in *Proc. Int. Conf. Electr. Mach. (ICEM)*, Sep. 2022, pp. 1498–1504.

[11] J. K. Tangudu and T. M. Jahns, "Comparison of interior PM machines with concentrated and distributed stator windings for traction applications," in *Proc. IEEE Vehicle Power Propuls. Conf.*, Sep. 2011, pp. 1–8.

[12] X. Chen, H. Fang, D. Li, R. Qu, X. Fan, and H. Hu, "Suppression of winding AC losses in high-speed permanent magnet machines by novel transposition technologies," in *Proc. IEEE Energy Convers. Congr. Expo. (ECCE)*, Oct. 2021, pp. 4539–4545.

[13] A. Mlot, M. Lukaniszyn, and M. Kokosz, "Analysis of end-winding proximity losses in a high-speed PM machine," in *Proc. Selected Problems Elect. Eng. Electron. (WZEE)*, vol. 65, no. 2, Jan. 2015, pp. 249–261, doi: 10.1515/aee-2016-0017.

[14] R. Wrobel and B. Mecrow, "A comprehensive review of additive manufacturing in construction of electrical machines," *IEEE Trans. Energy Convers.*, vol. 35, no. 2, pp. 1054–1064, Jun. 2020.

[15] B. AC. (Nov. 27, 2019). *Additive Manufacturing: 3D Printing to Perfection*. BMW AG. [Online]. Available: https://www.bmw.com/en/innovation/3d-print.html

[16] N. Simpson, J. Jung, A. Helm, and P. Mellor, "Additive manufacturing of a conformal hybrid-strand concentrated winding topology for minimal AC loss in electrical machines," in *Proc. IEEE Energy Convers. Congr. Expo. (ECCE)*, Vancouver, BC, Canada, Oct. 2021, pp. 3844–3851.

[17] X. Zhao, Z. Sun, and Y. Xu, "Multi-objective optimization design of permanent magnet synchronous motor based on genetic algorithm," in *Proc. 2nd Int. Conf. Mach. Learn., Big Data Bus. Intell. (MLBDBI)*, Oct. 2020, pp. 405–409.

[18] L. Piscini, D. Matt, A. Gimeno, and N. Boubaker, "Contribution on AC bar windings losses reduction for a high frequency and high performance machine for aeronautical application," in *Proc. 19th Int. Symp. Electromagn. Fields Mechatronics, Electr. Electron. Eng. (ISEF)*, Aug. 2019, pp. 1–3.

[19] D. Pan, L. Li, and M. Wang, "Modeling and optimization of air-core monopole linear motor based on multiphysical fields," *IEEE Trans. Ind. Electron.*, vol. 65, no. 12, pp. 9814–9824, Dec. 2018.

[20] X. Ren, A. Thabuis, and Y. Perriard, "Innovative design of 3D-printed winding for linear motor," in *Proc. 25th Int. Conf. Electr. Mach. Syst. (ICEMS)*, Nov. 2022, pp. 1–6.

[21] M. J. Akhtar and R. K. Behera, "Optimal design of stator and rotor slot of induction motor for electric vehicle applications," *IET Electr. Syst. Transp.*, vol. 9, no. 1, pp. 35–43, Mar. 2019.

[22] F. Wu and A. M. EL-Refaie, "Toward additively manufactured electrical machines: Opportunities and challenges," *IEEE Trans. Ind. Appl.*, vol. 56, no. 2, pp. 1306–1320, Mar. 2020.

[23] A. Selema, M. N. Ibrahim, and P. Sergeant, "Additively manufactured ultralight shaped-profile windings for HF electrical machines and weight-sensitive applications," *IEEE Trans. Transport. Electrific.*, vol. 8, no. 4, pp. 4313–4324, Dec. 2022.

[24] P. Lindh, H. Jussila, J. Pyrhonenl, and A. Parviainen, "Concentrated wound PM motors with semi-closed slots and with open slots," *Int. Rev. Elect. Eng.*, vol. 5, no. 2, pp. 491–497, 2010.

[25] J. Shier and P. Bourke, "An algorithm for random fractal filling of space," *Comput. Graph. Forum*, vol. 32, no. 8, pp. 89–97, Dec. 2013.

[26] F. Kiani and H. Tahanian, "A new methodology for design optimization of interior permanent magnet motors for electric vehicle applications," in *Proc. 3rd Int. Conf. Electr. Mach. Drives (ICEMD)*, Dec. 2023, pp. 1–5.

[27] D. Liang, Z. Q. Zhu, Y. Zhang, J. Feng, S. Guo, Y. Li, J. Wu, and A. Zhao, "A hybrid lumped-parameter and two-dimensional analytical thermal model for electrical machines," *IEEE Trans. Ind. Appl.*, vol. 57, no. 1, pp. 246–258, Jan. 2021.

[28] L. Jin, Y. Mao, X. Wang, L. Lu, and Z. Wang, "A model-based and data-driven integrated temperature estimation method for PMSM," *IEEE Trans. Power Electron.*, vol. 39, no. 7, pp. 8553–8561, Jul. 2024.

[29] R. Reddivari, V. Savant, and H. Eldeeb, "A model-based lumped parameter thermal network for online temperature estimation of IPMSM in automotive applications," in *Proc. IEEE Int. Transp. Electrific. Conf. (ITEC-India)*, India, Chennai, Dec. 2023, pp. 1–6.

[30] *Methods for Optimisation and Robustness Analysis*, Dynardo GmbH, Weimar, Germany, 2020.

[31] T. Most and J. Will, "Metamodel of optimal prognosis—An automatic approach for variable reduction and optimal meta-model selection," *Weimar: Res. Gate*, vol. 5, pp. 1–21, Nov. 2008.

[32] N. Riviere, M. Stokmaier, and J. Goss, "An innovative multi-objective optimisation approach for the multiphysics design of electrical machines," in *Proc. Transp. Electrific. Conf. Expo (ITEC)*, Jun. 2020, pp. 691–696.

[33] G. Petrelli, S. Nuzzo, D. Barater, T. Zou, G. Franceschini, and C. Gerada, "Preliminary sensitivity analysis and optimisation of a wound field synchronous motor for traction applications," in *Proc. AEIT Int. Conf. Electr. Electron. Technol. Automot. (AEIT AUTOMOTIVE)*, Modena, Italy, Jul. 2023, pp. 1–6.

[34] T. Helmholdt-Zhu and H. Borcherding, "Investigations on the influences of winding positions and rise times on the winding isolation system within the line-end coil under fast rising impulse voltages," in *Proc. 23rd Eur. Conf. Power Electron. Appl. (EPE ECCE Eur.)*, Sep. 2021, pp. 1–10.

[35] E. Roshandel, N. Ertugrul, A. Mahmoudi, and S. Kahourzade, "Design optimisation of a high power density electric machine using soft magnetic composites," in *Proc. 32nd Australas. Universities Power Eng. Conf. (AUPEC)*, Sep. 2022, pp. 1–6.

[36] F. Yu, H. Chen, W. Yan, V. F. Pires, J. F. A. Martins, P. Rafajdus, A. Musolino, L. Sani, M. P. Aguirre, M. A. Saqib, M. Orabi, and X. Li, "Design and multiobjective optimization of a double-stator axial flux SRM with full-pitch winding configuration," *IEEE Trans. Transport. Electrific.*, vol. 8, no. 4, pp. 4348–4364, Dec. 2022.

[37] J. Li, Y. Li, and Y. Wang, "Fuzzy inference NSGA-III algorithm-based multi-objective optimization for switched reluctance generator," *IEEE Trans. Energy Convers.*, vol. 36, no. 4, pp. 3578–3581, Dec. 2021.

[38] A. Selema, M. N. Ibrahim, R. Sprangers, and P. Sergeant, "Effect of using different types of magnet wires on the AC losses of electrical machine windings," in *Proc. IEEE Int. Electr. Mach. Drives Conf. (IEMDC)*, May 2021, pp. 1–5.

[39] J. McKay, J. Miscandlon, and T. Konkova, "The Design and optimisation of additively manufactured windings utilising data driven algorithms for minimal loss in electric machines," *IEEE Access*, vol. 12, pp. 187406–187426, 2024.

[40] J. Robinson, S. P. Munagala, A. Arjunan, N. Simpson, R. Jones, A. Baroutaji, L. T. Govindaraman, and I. Lyall, "Electrical conductivity of additively manufactured copper and silver for electrical winding applications," *Materials*, vol. 15, no. 21, p. 7563, Oct. 2022.

[41] C. Silbernagel, I. Ashcroft, P. Dickens, and M. Galea, "Electrical resistivity of additively manufactured AlSi10Mg for use in electric motors," *Additive Manuf.*, vol. 21, pp. 395–403, May 2018.

[42] P. A. Lykov, E. V. Safonov, and A. M. Akhmedianov, "Selective laser melting of copper," *Mater. Sci. Forum*, vol. 843, pp. 284–288, Feb. 2016.

[43] J. P. Kruth, X. Wang, T. Laoui, and L. Froyen, "Laser and materials in selective laser sintering," *Assembly Autom.*, vol. 23, pp. 357–371, Dec. 2003.

[44] S. R. Pogson, P. Fox, C. J. Sutcliffe, and W. O'Neill, "The production of copper parts using DMLR," *Rapid Prototyping J.*, vol. 9, no. 5, pp. 334–343, Dec. 2003.

[45] T. Husain, C. Ma, N. Taran, and Z. Wan, "A comprehensive comparison of concentrated winding and distributed continous winding machine topologies for hybrid electric vehicles," in *Proc. IEEE Energy Convers. Congr. Expo.*, Vancouver, BC, Canada, Oct. 2021, pp. 3683–3689.

[46] F. Wu, A. M. EL-Refaie, and A. Al-Qarni, "Additively manufactured hollow conductors integrated with heat pipes: Design tradeoffs and hardware demonstration," *IEEE Trans. Ind. Appl.*, vol. 57, no. 4, pp. 3632–3642, Jul. 2021.

[47] N. Simpson, D. J. North, S. M. Collins, and P. H. Mellor, "Additive manufacturing of shaped profile windings for minimal AC loss in electrical machines," *IEEE Trans. Ind. Appl.*, vol. 56, no. 3, pp. 2510–2519, May 2020.

[48] W. H. Kan, Y. Nadot, M. Foley, L. Ridosz, G. Proust, and J. M. Cairney, "Factors that affect the properties of additively-manufactured AlSi10Mg: Porosity versus microstructure," *Additive Manuf.*, vol. 29, Oct. 2019, Art. no. 100805.

[49] P. Shubham, A. Sharma, P. N. Vishwakarma, and R. K. Phanden, "Predicting strength of selective laser melting 3D printed A1Si10Mg alloy parts by machine learning models," in *Proc. 8th Int. Conf. Signal Process. Integr. Netw. (SPIN)*, Aug. 2021, pp. 745–749.

[50] S. Vahid, T. Chowdhury, S. Koushan, and A. El-Refaie, "Electrical characteristics of additively manufactured hollow conductor coils with integrated heat pipes for electric aircraft applications," in *Proc. IEEE Energy Convers. Congr. Expo. (ECCE)*, Oct. 2022, pp. 1–8.

[51] M. Sarap, A. Kallaste, P. S. Ghahfarokhi, H. Tiismus, and T. Vaimann, "The effect of build direction on the thermal conductivity of additively manufactured AlSi10Mg and silicon-steel samples," in *Proc. Int. Conf. Electr. Mach. (ICEM)*, Sep. 2022, pp. 538–543.

[52] P. Yang, L. A. Deibler, D. R. Bradley, D. K. Stefan, and J. D. Carroll, "Microstructure evolution and thermal properties of an additively manufactured, solution treatable AlSi10Mg," *J. Mater. Res.*, vol. 33, pp. 1–13, Nov. 2018.

[53] *Electronics Materials Solutions Division, 3M*, 3M Polyimide Film Tape 5413, 3M, St Paul, MI, USA, 2021, pp. 1–3.

[54] M. Price and E. Butts, "Troubleshooting three-phase electric motors," *Water Well J.*, Apr. 2022.

[55] A. Mostafaei, A. M. Elliott, J. E. Barnes, F. Li, W. Tan, C. L. Cramer, P. Nandwana, and M. Chmielus, "Binder jet 3D printing—Process parameters, materials, properties, modeling, and challenges," *Prog. Mater. Sci.*, vol. 119, Jun. 2021, Art. no. 100707.

[56] H. Sonar, S. Ghosh, R. Kr. Singh, V. Khanzode, M. Akarte, and N. Ghag, "Implementing additive manufacturing for sustainability in operations: Analysis of enabling factors," *IEEE Trans. Eng. Manag.*, vol. 71, pp. 1–15, Sep. 2022.

[57] H. Gupta, J. N. Lawal, I. J. Orji, and S. Kusi-Sarpong, "Closing the gap: The role of distributed manufacturing systems for overcoming the barriers to manufacturing sustainability," *IEEE Trans. Eng. Manag.*, vol. 70, no. 5, pp. 1754–1773, May 2023.

[58] A. Gunasekaran and A. Spalanzani, "Sustainability of manufacturing and services: Investigations for research and applications," *Int. J. Prod. Econ.*, vol. 140, no. 1, pp. 35–47, Nov. 2012.

[59] C. Bai, P. Dallasega, G. Orzes, and J. Sarkis, "Industry 4.0 technologies assessment: A sustainability perspective," *Int. J. Prod. Econ.*, vol. 229, Nov. 2020, Art. no. 107776.

[60] V. Alcácer and V. Cruz-Machado, "Scanning the Industry 4.0: A literature review on technologies for manufacturing systems," *Eng. Sci. Technol., Int. J.*, vol. 22, no. 3, pp. 899–919, Jun. 2019.

[61] D. Kolberg and D. Zühlke, "Lean automation enabled by Industry 4.0 technologies," *IFAC-PapersOnLine*, vol. 48, no. 3, pp. 1870–1875, 2015.

[62] L. Damiani, M. Demartini, G. Guizzi, R. Revetria, and F. Tonelli, "Augmented and virtual reality applications in industrial systems: A qualitative review towards the Industry 4.0 era," *IFAC-PapersOnLine*, vol. 51, no. 11, pp. 624–630, 2018.

[63] E. A. Alaref and S. A. Khan, "Industry 4.0 and its technologies: A systematic literature review," in *Proc. IEEE Int. Conf. Ind. Eng. Eng. Manage. (IEEM)*, Singapore, Dec. 2021, pp. 1004–1009.

[64] G. R. Mitchell, "Climate change and manufacturing," *Proc. Manuf.*, vol. 12, pp. 298–306, Jan. 2017.

[65] P. Kumar, R. K. Singh, and V. Kumar, "Managing supply chains for sustainable operation in the era of industry 4.0 and circular economy: Analysis of barriers," *Resour., Conservation Recycling*, vol. 164, Jan. 2021, Art. no. 105215.
[66] R. Agrawal, "Sustainable design guidelines for additive manufacturing applications," *Rapid Prototyping J.*, vol. 28, no. 7, pp. 1221–1240, Jun. 2022.
[67] A. Ghobadian, I. Talavera, A. Bhattacharya, V. Kumar, J. A. Garza-Reyes, and N. O'Regan, "Examining legitimatisation of additive manufacturing in the interplay between innovation, lean manufacturing and sustainability," *Int. J. Prod. Econ.*, vol. 219, pp. 457–468, Jan. 2020.
[68] S. Ford and M. Despeisse, "Additive manufacturing and sustainability: An exploratory study of the advantages and challenges," *J. Cleaner Prod.*, vol. 137, pp. 1573–1587, Nov. 2016.
[69] K. Kuzmenko, N. Ducoulombier, A. Feraille, and N. Roussel, "Environmental impact of extrusion-based additive manufacturing: Generic model, power measurements and influence of printing resolution," *Cement Concrete Res.*, vol. 157, Jul. 2022, Art. no. 106807.
[70] H. Wu, H. Mehrabi, N. Naveed, and P. Karagiannidis, "A business model for additive manufacturing of recycled plastics towards sustainability," *Int. J. Adv. Manuf. Technol.*, vol. 120, nos. 11–12, pp. 7997–8011, Jun. 2022.
[71] A. Iqbal, G. Zhao, H. Suhaimi, N. He, G. Hussain, and W. Zhao, "Readiness of subtractive and additive manufacturing and their sustainable amalgamation from the perspective of Industry 4.0: A comprehensive review," *Int. J. Adv. Manuf. Technol.*, vol. 111, nos. 9–10, pp. 2475–2498, Dec. 2020.
[72] M. Rinaldi, M. Caterino, M. Fera, P. Manco, and R. Macchiaroli, "Technology selection in green supply chains–the effects of additive and traditional manufacturing," *J. Cleaner Prod.*, vol. 282, Feb. 2021, Art. no. 124554.
[73] M. K. Niaki, F. Nonino, G. Palombi, and S. A. Torabi, "Economic sustainability of additive manufacturing: Contextual factors driving its performance in rapid prototyping," *J. Manuf. Technol. Manage.*, vol. 30, no. 2, pp. 353–365, Feb. 2019.
[74] T. Pereira, J. V. Kennedy, and J. Potgieter, "A comparison of traditional manufacturing vs additive manufacturing, the best method for the job," *Proc. Manuf.*, vol. 30, pp. 11–18, Jan. 2019.
[75] K. Kellens, R. Mertens, D. Paraskevas, W. Dewulf, and J. R. Duflou, "Environmental impact of additive manufacturing processes: Does AM contribute to a more sustainable way of part manufacturing?" *Proc. CIRP*, vol. 61, pp. 582–587, Jan. 2017.
[76] S. Kokare, J. P. Oliveira, and R. Godina, "Life cycle assessment of additive manufacturing processes: A review," *J. Manuf. Syst.*, vol. 68, pp. 536–559, Jun. 2023.
[77] F. Psarommatis, J. Sousa, J. P. Mendonça, and D. Kiritsis, "Zero-defect manufacturing the approach for higher manufacturing sustainability in the era of Industry 4.0: A position paper," *Int. J. Prod. Res.*, vol. 60, no. 1, pp. 73–91, Jan. 2022.
[78] P. C. Priarone, V. Lunetto, E. Atzeni, and A. Salmi, "Laser powder bed fusion (L-PBF) additive manufacturing: On the correlation between design," *Proc. CIRP*, vol. 78, pp. 85–90, Jan. 2018.
[79] H. P. N. Nagarajan and K. R. Haapala, "Characterizing the influence of resource-energy-exergy factors on the environmental performance of additive manufacturing systems," *J. Manuf. Syst.*, vol. 48, pp. 87–96, Jul. 2018.
[80] W. Davis, V. Lunetto, P. C. Priarone, D. Centea, and L. Settineri, "An appraisal on the sustainability payback of additively manufactured molds with conformal cooling," *Proc. CIRP*, vol. 90, pp. 516–521, Jan. 2020.
[81] S. Guarino, G. S. Ponticelli, and S. Venettacci, "Environmental assessment of selective laser melting compared with laser cutting of 316L stainless steel: A case study for flat washers' production," *CIRP J. Manuf. Sci. Technol.*, vol. 31, pp. 525–538, Nov. 2020.
[82] J. Faludi, C. Bayley, S. Bhogal, and M. Iribarne, "Comparing environmental impacts of additive manufacturing vs traditional machining via life-cycle assessment," *Rapid Prototyping J.*, vol. 21, no. 1, pp. 14–33, Jan. 2015.
[83] A. Vevers, A. Kromanis, E. Gerins, and J. Ozolins, "Additive manufacturing and casting technology comparison: Mechanical properties, productivity and cost benchmark," *Latvian J. Phys. Tech. Sci.*, vol. 55, no. 2, pp. 56–63, Apr. 2018.
[84] M. Gröninger, F. Horch, A. Kock, M. Jakob, and B. Ponick, "Cast coils for electrical machines and their application in automotive and industrial drive systems," in *Proc. 4th Int. Electr. Drives Prod. Conf. (EDPC)*, Sep. 2014, pp. 1–7.
[85] J.-W. Chin, K.-S. Cha, E.-C. Lee, S.-H. Park, J.-P. Hong, and M.-S. Lim, "Design of PMSM for EV traction using MSO coil considering AC resistance according to current density and parallel circuit," in *Proc. IEEE Vehicle Power Propuls. Conf. (VPPC)*, Oct. 2019, pp. 1–6.
[86] A. Gneiting, M. Waldhof, and N. Parspour, "A systematic design methodology based on data clustering for automotive drive cycle oriented optimization of electrically excited synchronous machines," in *Proc. IEEE 7th Southern Power Electron. Conf. (SPEC)*, Dec. 2022, pp. 1–8.

JOHN MCKAY (Member, IEEE) received the M.Eng. degree in electronics and electrical engineering from the University of Strathclyde, Glasgow, U.K., in 2015. He is currently pursuing the Ph.D. degree. He is also an Engineer with the Department of Design, Manufacturing and Engineering Management and the Advanced Forming Research Centre, University of Strathclyde. His research belongs to the Future Electric Machines Manufacturing (FEMM) hub, an EPSRC-funded venture with the National Manufacturing Institute Scotland (NMIS). His research interests include the improvement of the performance of electrical machines through the use of advanced multi-physics, algorithmic design processes, and novel manufacturing techniques utilizing additive manufacturing of active components for potential deployments in automotive, aerospace, transportation, and manufacturing.

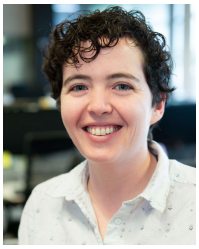

JILL MISCANDLON graduated from the University of Strathclyde with a PhD and BSC (Hons) in mathematics before joining the Advanced Forming Research Centre, a technical centre within National Manufacturing Institute Scotland. She worked for six years leading large-scale collaborative research and development (CR&D) projects on novel forming processes, such as flow forming and spinning, including the (Strategic Affordable Manufacturing in U.K. through Leading Environmental Technologies (SAMULET) and Manufacturing Portfolio projects. She is currently leading two grand challenges for the EPSRC's Future Electrical Machines Manufacturing Hub, including developing the work package around sustainable manufacture and circular economy of electrical machines. Her research interests include manufacturing innovations for electrical machines, near-net shape-forming technologies, and sustainable manufacture and design.

TATYANA KONKOVA is currently a Senior Lecturer, leading the Materials Processing Team, Department of Design, Manufacturing and Engineering Management (DMEM), University of Strathclyde (UoS). She has significant expertise in advanced materials characterization techniques, materials thermo-mechanical behaviors, electropulse treatment, electrodeposition, and additive manufacturing. She has over 50 highly cited publications and has authored numerous industrial reports. She has led research and knowledge exchange programs focused on materials behavior during forging, forming, and processing. She is a Chartered Engineer, a member of IMechE and The Scottish Association for Metals (SAM) Council, and a Fellow of IOM3.